International Journal of Solids and Structures 129 (2017) 195–203

Contents lists available at ScienceDirect

International Journal of Solids and Structures

journal homepage: www.elsevier.com/locate/ijsolstr

The creep of alloy 617 at 700 °C: Material properties, measurement of strain and comparison between finite element analysis and digital image correlation

A. Narayanan*, K. Dubey, C.M. Davies, J.P. Dear

Department of Mechanical Engineering, Imperial College London, South Kensington Campus, London, SW7 2AZ, United Kingdom

ARTICLE INFO

Article history:
Received 8 April 2017
Revised 27 July 2017
Available online 24 August 2017

Keywords:
Creep
Alloy 617
Multiaxial stress state
Finite element studies

ABSTRACT

Future generations of power plants, such as the Ultra-Super-Critical (USC) power plants, are being designed to be operated at more extreme pressures and temperatures in order to achieve higher efficiency. One candidate material for components is Inconel alloy grade 617, a nickel based superalloy, which is expected to possess better creep resistance in comparison to other types of alloys (Bhadeshia and Honeycombe, 2011; Evans and Wilshire, 1993). At present there is little available data or information about the behaviour of this material at the temperature of interest (700 °C) and hence there is a need to evaluate its properties under these conditions.

This paper details experimentation on Alloy 617 to evaluate its uniaxial behaviour under tension and creep at 700 °C, using the results obtained to develop a creep damage model based on power law creep in conjunction with the Cocks–Ashby void growth approach Cocks and Ashby (1982) for creep in a multiaxial stress state. Finite Element (FE) simulations are compared to experimental results obtained by Digital Image Correlation (DIC), which is used in order to validate the effectiveness of a power law creep damage model. Results made using a novel electrical strain sensor using ACPD principles supplement this work to draw comparisons between the response of the sensor and the strain field experienced by the specimen.

1. Introduction

Alloy 617 (also known as Inconel alloy 617) is a nickel-chromium based superalloy, composing of at least 44.5% nickel and 20% chromium (composition can be found in Inconel alloy 617). Superalloys are a class of material with superior performance at elevated temperatures to conventional alloys, leading them to be popular for use in both aerospace and power generation applications, usually in the manufacture of turbine blades.

Alloy 617 is known for good oxidation resistance and creep strength up to 1093 °C, and its room temperature tensile properties have been observed to improve significantly upon 1000 hours exposure to temperatures between 649 °C and 870 °C (Mankins et al., 1974). Most of the existing literature concerns its usage at temperatures well above those in plant condition and limited data exists on its properties. Recently, long term tests have been performed to determine creep properties of specimens extracted from thick-walled pipes (Knezevic et al., 2013), while work has shown that modifying alloy 617 by adding more boron up to 60 ppm increases its creep rupture strength (Klöwer et al., 2013). Nevertheless, there remains much more work to be done in order to obtain a detailed understanding of its behaviour.

In practice, components consist of networks of material joined by welds and which may have varying geometric features along the length. Consequently they are more likely to experience a multiaxial stress state. Hence, data obtained from the uniaxial experiments is used in conjunction with typical power law creep models to model the deformation of a double-edged notch tension (DENT) specimen, where the notch simulates the presence of a stress raiser such as a defect or a weld. The suitability of the creep models for Alloy 617 is tested using two DENT specimens whose behaviour is experimentally analysed using Digital Image Correlation (DIC), a method that allows the strain field over the surface of a specimen to be determined. Research has been performed using DIC to investigate the creep of a DENT specimen, showing its usefulness as

* Corresponding author. Present Address: Department of Mechanical Engineering, University of Bristol, Queen's Building, University Walk, Bristol, BS8 1TR, England.
E-mail addresses: a.narayanan@bristol.ac.uk (A. Narayanan), kanishkdubey@hotmail.com (K. Dubey), catrin.davies@imperial.ac.uk (C.M. Davies), j.dear@imperial.ac.uk (J.P. Dear).

http://dx.doi.org/10.1016/j.ijsolstr.2017.08.021

a tool to measure creep strain (Gariboldi et al., 2016) albeit at significantly lower temperatures than those considered here.

This body of research has three complementary aims. The first is to measure and calculate mechanical properties of Alloy 617 at 700 °C experimentally, with particular focus on uniaxial tensile and creep properties. This data is then used to evaluate creep constants for simulating the behaviour of the material. The importance of this is to establish an understanding of how it behaves at 700 °C.

The second aim is to determine whether creep strain accumulated by specimens of Alloy 617 at this temperature can be accurately measured in-situ using a novel alternating current potential drop (ACPD) strain sensor (Prajapati et al., 2012; Madhi and Nagy, 2011c; Davies et al., 2011). This is essential as it enables the condition of the component material to be evaluated easily.

Finally, the third aim is to ascertain whether power law models for creep deformation provide an accurate prediction of the behaviour of Alloy 617, particularly when subject to a multiaxial stress field. This is critical to ensure that the typical models used within the field are appropriate.

2. Mechanics of creep deformation

Creep is generally modelled through various uses of power-law models to represent the relationship between different quantities. A representation of the entire creep curve of a material can be made using Eq. (1), combining the effects of all three stages of creep into one expression

$$\dot{\varepsilon}_a = A_a \sigma^{n_a} \tag{1}$$

where $\dot{\varepsilon}_a$ is the average creep strain rate, A_a is the average creep coefficient and n_a is the average creep stress index.

Similarly the secondary or minimum creep strain rate ($\dot{\varepsilon}_s$) can be represented using a power law expression of the form of Eq. (2),

$$\dot{\varepsilon}_s = A_s \sigma^{n_s} \tag{2}$$

where A_s and n_s are the secondary creep coefficient and secondary creep stress index respectively.

The various values of A and n are determined by regression fits to uniaxial creep data. In addition, if stress is plotted against time to rupture it also obeys a power law relationship given by Eq. (3)

$$t_f = B_r \sigma^{\nu_r} \tag{3}$$

where B_r and ν_r are constants to be found. This relationship can be used to predict the rupture behaviour of the material.

2.1. Modelling creep behaviour

The finite element (FE) model used to simulate the behaviour of Alloy 617 incorporates an elastic-plastic analysis of the material behaviour during loading (obtained from results presented within this paper), and simulates creep using the average creep strain rate properties determined within this research (see Table 5). The effect of creep damage is modelled using ductility exhaustion concepts as per Eq. (4)

$$\omega = \frac{\varepsilon_c}{\varepsilon_f} \tag{4}$$

where ω is the damage, ε_c is the amount of creep strain predicted by the creep law used and ε_f is the uniaxial creep failure strain measured from uniaxial creep tests. The damage parameter, ω, is defined such that $0 \leq \omega \leq 1$ and failure occurs when ω approaches 1. The rate of damage accumulation, is related to the equivalent creep strain rate by the relationship in Eq. (5)

$$\dot{\omega} = \frac{\dot{\varepsilon}_c}{\varepsilon_f^*} \tag{5}$$

and the total damage at any instant is the integral of the damage rate in Eq. (5) thus given by

$$\omega = \int_0^t \dot{\omega} dt \tag{6}$$

In this body of work, the creep strain rate used is the average creep strain rate ($\dot{\varepsilon}_a$), and so it is taken that $\dot{\varepsilon}_c = \dot{\varepsilon}_a$.

The damage accumulation in a multiaxial stress state depends on the growth and coalescence of voids at grain boundaries. In the vicinity of the crack tip the local (multiaxial) creep ductility, ϵ_f^*, may be obtained for the material under study from the Cocks and Ashby (1982) model. The Cocks–Ashby model describes the evolution of creep damage due to the growth of voids at grain boundaries and is a typical model used for a variety of alloys (Spindler, 2004; Xu et al., 2016). Due to the limited amount of research on alloy 617 at 700 °C, the Cocks–Ashby model has been chosen due to its general wide use in the field.

The model describes the ratio of the multiaxial to uniaxial failure strain as a function of the triaxiality, h, as detailed in Eq. (7)

$$\frac{\varepsilon_f^*}{\varepsilon_f} = \frac{\sinh[\frac{2}{3}(\frac{n-0.5}{n+0.5})]}{\sinh[2(\frac{n-0.5}{n+0.5})h]} \tag{7}$$

where n is whichever stress index has been used in the calculation of steady state creep (either n_a or n_s). The triaxiality describes the stress state present within the material as the ratio of the mean stress to the von Mises equivalent stress (i.e. $h = \sigma_m/\sigma_{vm}$).

When a portion of material becomes fully damaged ($\omega = 0.999$, to avoid numerical problems) as described Eq. (4), it no longer has the ability to take the load. Thus it is assumed that the stress components in all directions will be zero in the elements concerned, which is simulated in a similar manner to Yatomi et al. (2004), Oh et al. (2011), Kim et al. (2013) and Mehmanparast et al. (2014) whereby the material properties of the damaged element (i.e. its stiffness) are reduced to a near-zero value.

A one-eighth model was constructed, as the presence of planes of symmetry in all three orthogonal directions meant that symmetry conditions could be applied to faces in each direction. Hence, it was possible to minimise the model size and therefore the number of elements within. A mesh refinement study showed that an element size of 62.5 μm at the notch root gave results of comparable accuracy and much shorter solving time to a more refined mesh. Elements were 8 node, linear brick elements, and the final mesh used around the notch is shown in Fig. 1.

Results are expressed as quantities measured along the notch throat, schematically shown in Fig. 2. The distance along the throat, r, is normalised with respect to the distance between the notch root and the longitudinal centreline of the specimen, a.

3. Material property determination

A section of curved Alloy 617 piping, 350 mm in length was provided, and is shown in Fig. 3. After fabrication the pipe had been annealed at 902 °C for 50 min before being cooled by water. It was then subject to a temperature of 700 °C for approximately 17,000 h. The chemical composition of this particular pipe was provided by the supplier, and is listed in Table 1.

3.1. Tensile properties

Three cylindrical bar specimens of 8 mm diameter were loaded in tension to failure in a tensile testing machine, one at room temperature and two at 700 °C. Displacement was measured using an Instron 2620-601 clip-on extensometer in room temperature tests or a Linear Variable Differential Transducer (LVDT) at high temperature, and used to calculate strain. In the tensile test performed at

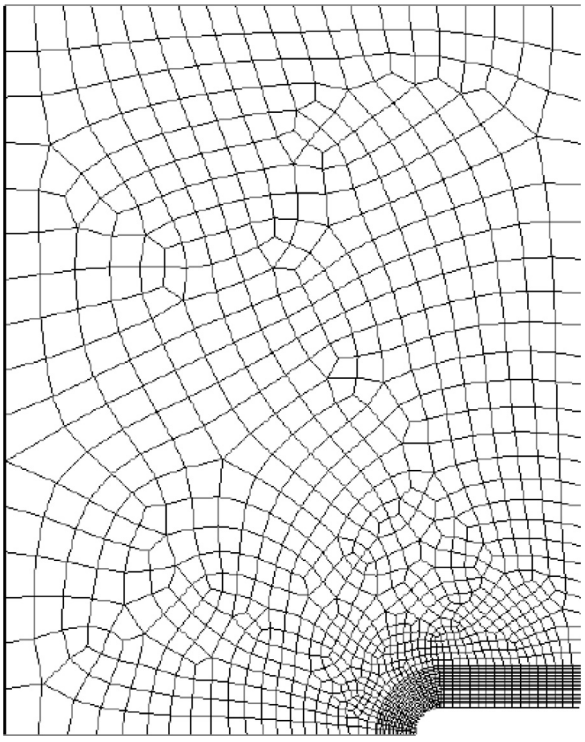

Fig. 1. Cross-section of specimen geometry used in FE model of DENT specimen, showing mesh on cross-section of 3D model.

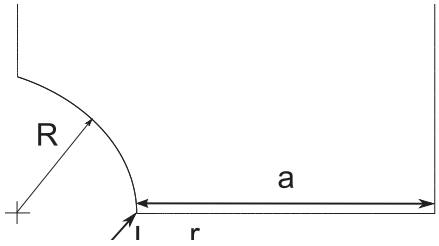

Fig. 2. Co-ordinate scheme used in expressing results over the throat of notched specimens.

Fig. 3. Section of Alloy 617 piping used for experimentation (shown alongside A4 sheet of paper as size comparison).

700 °C, the specimen temperature was monitored using thermocouples attached according to ASTM Standard E633 (ASTM International, 2005).

3.2. Creep properties

In order to determine the creep properties of Alloy 617, a series of six uniaxial creep tests at 700 °C were performed. Tests involved first exposing the specimens to a uniform temperature field at 700 °C, which was measured using thermocouples attached on different parts of the specimen according to the aforementioned ASTM Standard E633 (ASTM International, 2005). This temperature field was held for 24 h to ensure that it remained constant before a constant load, applied using dead weights, was applied to the specimen. Each specimen was tested at a different load and allowed to creep until failure so as to obtain the material's response over a range of stresses.

Stress is expressed as the net section stress according to Eq. (8)

$$\sigma = \frac{W}{A_0} \tag{8}$$

where W is the applied load and A_0 is the initial cross-sectional area of the gauge region of the specimen. Loads were varied to give an applied stress from 270 to 340 MPa and rupture times in excess of 100 h. Strain calculated from the extension of the gauge region of the specimen measured using a Linear Variable Differential Transducer (LVDT). LVDTs were calibrated after each test in order to obtain an accurate displacement-voltage characteristic.

Table 1
Chemical composition of Alloy 617 pipe material provided (by % wt.)

Ni	Cr	Co	Mo	C	Si	Al	Fe	Ti
54.27	22.34	11.70	9.26	0.06	0.06	0.97	0.87	0.43

4. Creep monitoring systems

4.1. Digital image correlation

Digital Image Correlation (DIC) is an optical method of measuring strain over an area on the surface of a material. It uses a random pattern of paint specks painted on the surface of the test subject and a camera system to capture images while it undergoes loading. By tracking and comparing progressive images during deformation, strain can be mapped across the surface.

Using a furnace with a porthole, a Single Lens Reflex (SLR) camera was positioned to be able to take pictures of the specimen surface during creep. High temperature paint capable of withstanding over 1000 °C was sprayed over the specimen surface to apply the speckle pattern.

Facet sizes were between 70 × 70 pixels and 100 × 100 pixels, with facet overlap being between 20 and 40 pixels. Facet size and overlap were adjusted depending on the size of paint spots in the speckle pattern and in order to produce the smallest error. Errors in DIC measurement were determined by measuring the maximum fluctuation in reading at constant temperature with no loading (i.e. where no strain increase should occur), and error bars have been applied to each set of results in this manner.

4.2. The ACPD sensor

The ACPD sensor used involves a 2 × 2 square set of probes that measures the electrical resistance of the material. The principle of operation involves applying a low frequency current of 2 Hz into two probes and measuring the voltage across the other two, before doing the same in the orthogonal direction. As the component strains, the separation between the probes (and hence the resistance) increases in the direction of the load and decreases in the transverse direction. Therefore the change in resistance can be used to calculate the strain, meaning the sensor functions as a high temperature strain gauge, at least until local material effects such as crack formation become significant (Davies et al., 2011).

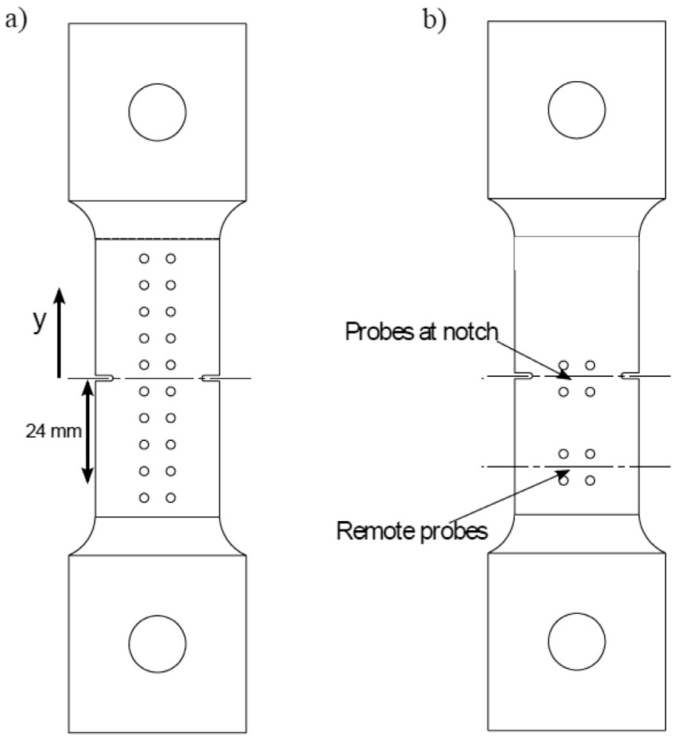

Fig. 4. Geometry of specimens tested with DIC and ACPD systems, showing schematics of a) specimen N-1 and b) specimen N-2.

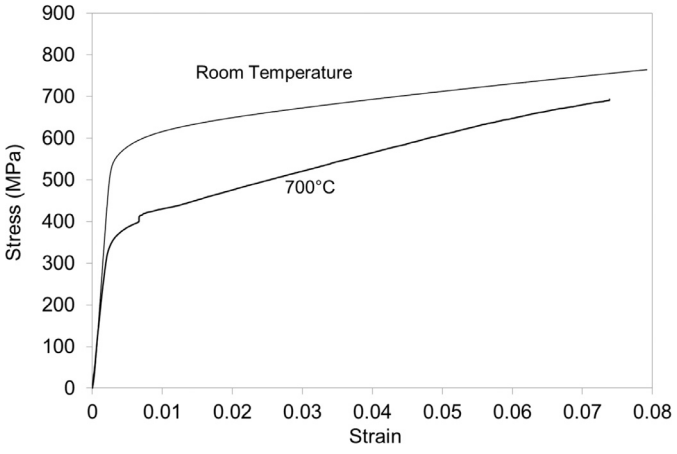

Fig. 5. True stress-true strain curves for Alloy 617 at room temperature and 700 °C.

Table 2
Tensile properties of Alloy 617 at room temperature.

Temperature	Elastic modulus, E (GPa)	0.2% Proof stress (MPa)	UTS (MPa)
Room Temperature	233	580	1253
700 °C	169	379	690

Results obtained are expressed as the ratio of the longitudinal resistance to the transverse resistance in order to negate effects of temperature. This resistance ratio is then normalised with respect to the initial measurement, producing a quantity called the *normalised resistance ratio* and given the symbol ξ.

The probes used in this sensor consist of stainless steel dowel pins welded to the surface of the specimen, with chromel wires attached to the pins to form the connection to the sensing units. A multiplexer switches between inputs, so measurements across multiple sets of probes can be made. An array of probes (2 × 10 long) has been applied along the gauge region of one DENT specimen, with two 2 × 2 sets affixed to the other one. The first configuration is designed to measure the variation in response progressively further away from the notch. These probe configurations are shown schematically in Fig. 4.

5. Results

5.1. Measurement of tensile properties

The stress-strain curves for Alloy 617 at both room temperature and 700 °C are shown in Fig. 5, with corresponding tensile properties given in Table 2. The elastic modulus at room temperature is greater than that quoted in Inconel alloy 617 by 10%, while both the 0.2% proof stress ($\sigma_{0.2}$) and ultimate tensile strength (UTS, σ_{UTS}) are significantly greater. At 700 °C, the effect of temperature has been to reduce both the proof stress and modulus, with the modulus at 700 °C being 76% the room temperature value and the 0.2% proof stress decreasing by 29.5%. Furthermore, the UTS at this temperature is just over half that at room temperature. When compared to the data sheet value (Inconel alloy 617), the former is 6% greater than the listed value of 166 GPa at 700 °C, which is to be expected when one considers that the room temperature experimental value of 233 GPa is 8% greater than the corresponding data sheet value.

5.2. Measurement of creep properties

Six uniaxial creep tests have been performed and are listed in Table 3. Strain-time histories for all specimens are plotted in Fig. 6, with strain calculated from displacement measured using a Linear Variable Differential Transducer (LVDT). It should be noted that the general trend for three of the specimens (tested at 325, 330 and 340 MPa) show very similar trends with a high degree of overlap. Indeed, the latter two specimens display almost exactly the same curve. The specimen tested at 325 MPa has failed before the specimens tested at 330 MPa and 340 MPa and accumulated half as much creep strain.

Results suggest that in this material, the creep ductility cannot be assumed to be constant over the stress range of the tests, which is borne out by Fig. 7a. The stress-rupture characteristic for the six completed tests is in Fig. 7b, with rupture properties displayed in Table 4.

Table 3
Details of testing on completed uniaxial creep specimens; $\dot{\varepsilon}_s$ is secondary creep strain rate and $\dot{\varepsilon}_a$ is average creep strain rate.

Stress (MPa)	Time to failure (h)	Failure strain (%)	$\dot{\varepsilon}_s$ (h^{-1})	$\dot{\varepsilon}_a$ (h^{-1})
270	2535	5.46	1.31×10^{-5}	2.12 × 10–5
279	1034	5.37	2.78×10^{-5}	5.23×10^{-5}
315	619	8.53	5.50×10^{-5}	1.38×10^{-4}
325	220	9.68	2.39×10^{-4}	4.41×10^{-4}
330	402	19.40	1.11×10^{-4}	4.83×10^{-4}
340	385	18.72	1.55×10^{-4}	4.86×10^{-4}

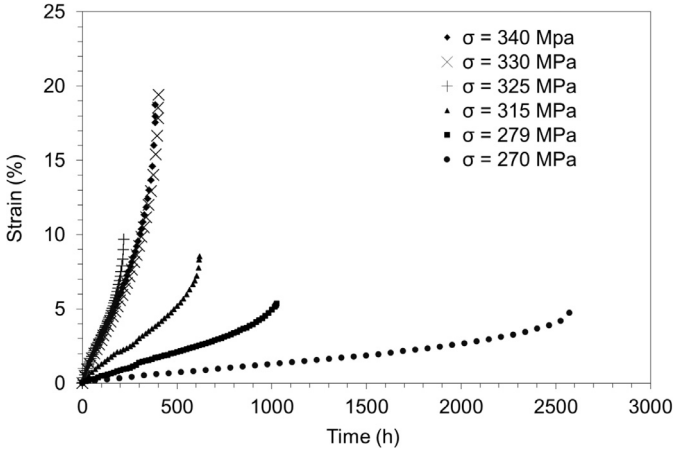

Fig. 6. Creep curves for uniaxial specimens of Alloy 617, identified in key by the magnitude of test stress, showing data at stresses of 340 MPa (diamonds), 330 MPa (crosses), 325 MPa (plus symbols), 315 (triangles), 279 MPa (squares) and 270 MPa (diamonds).

Table 4
Rupture constants for Alloy 617 at 700 °C.

Rupture stress index, ν_r	B_r ($MPa^{\nu_r}h$)
10.20	1.52×10^{28}

Table 5
Steady state creep constants using secondary and average creep strain rates for Alloy 617.

	Creep coefficient, A (MPa^{1/n_p})	Creep stress index, n
Secondary/minimum creep rate $\dot{\varepsilon}_s$ (h^{-1})	1.05×10^{-36}	12.85
Average creep rate $\dot{\varepsilon}_a$ (h^{-1})	1.72×10^{-38}	13.64

Table 6
Details of tests performed on DENT samples; σ_{net} is applied stress and $\sigma_{0.2}$ is the 0.2% proof stress.

Specimen	Temperature (°C)	σ_{net}	$\sigma_{net}/\sigma_{0.2}$	Test Duration (h)
N-1	700	300	0.73	194
N-2	700	300	0.73	577

The relationship between strain rate and applied stress determined from experiments is shown in Fig. 7c and d, and the creep constants derived are listed in Table 5 using a regression fit to the data on a set of logarithmic axes. Results have been plotted alongside results from similar work performed recently (Knezevic et al., 2013).

5.3. Measurement of creep strain

Two double-edged notch tension (DENT) specimens have been tested for the purpose of evaluating the capabilities of the ACPD sensor at 700 °C as well as observe the evolution of the strain field they experience, with conditions given in Table 6. Experiments

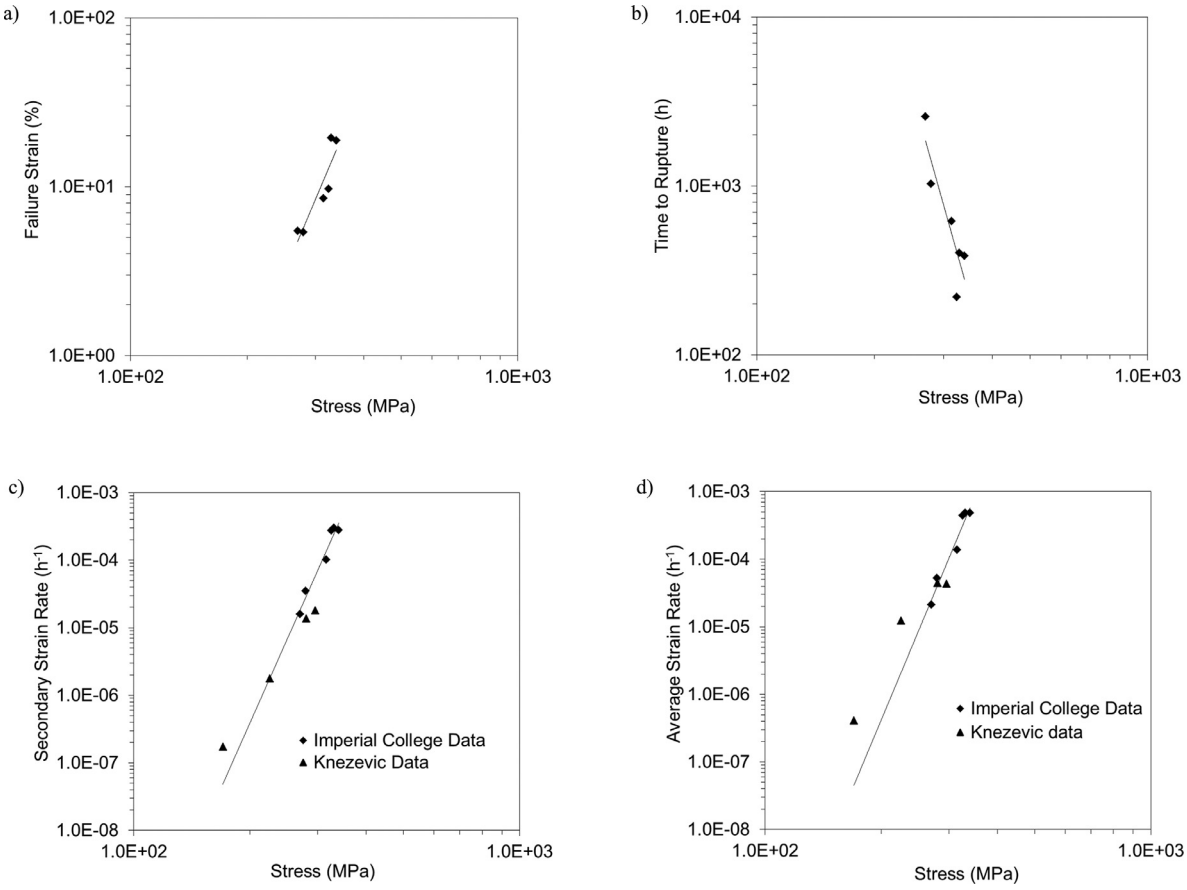

Fig. 7. Uniaxial creep properties for Alloy 617: a) Failure strain (ϵ_f) against stress (σ), b) Time to rupture (t_r) against stress c) Minimum creep rate against stress, d) Average creep rate against stress; Imperial College data (diamonds) as been plotted alongside Knezevic data (Knezevic et al., 2013) for c) and d) for comparison.

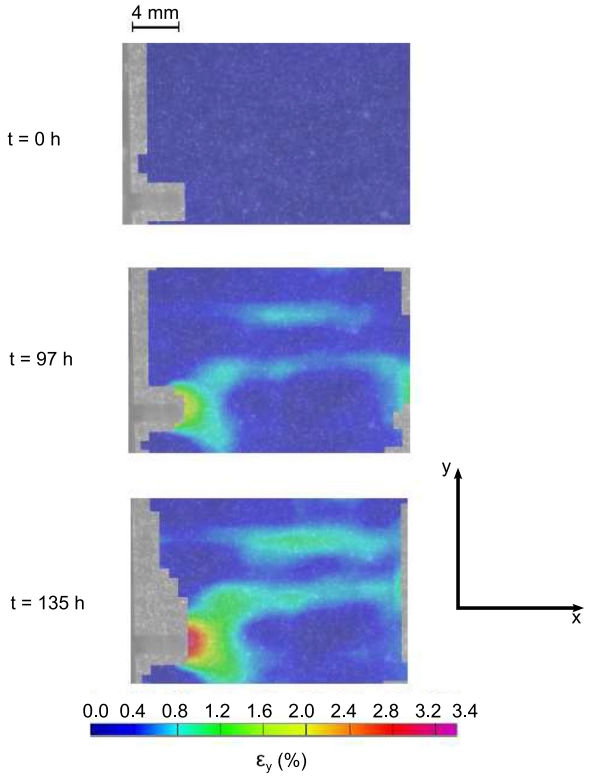

Fig. 8. Creep strain field evolution of specimen N-1: visualisation of the strain field using DIC overlaid on the image of the specimen at three points in time during the test.

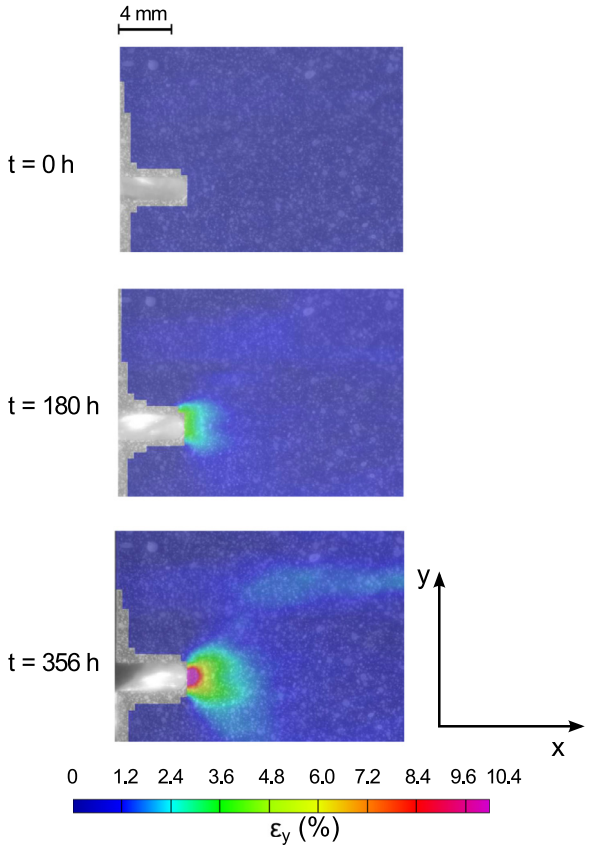

Fig. 9. Creep strain field evolution of specimen N-2: visualisation of the strain field using DIC overlaid on the image of the specimen at three points in time during the test; strain accumulation is much more localised in comparison to specimen N-1.

involved a similar setup to that specified in the previous section in terms of application of temperature and load. The sensors used are described in previous sections. Each specimen had a speckle pattern applied the surface facing the camera (through the porthole) and at least one set of four ACPD probes attached to the reverse side.

Before presenting the results for N-1 and N-2, it should be mentioned that although in Table 6 the time to failure is specified as 194 h and 577 h respectively, a large crack formed at one of the notches at 154 h in the case of the former and 479 h in the case of the latter. These cracks grew visibly until failure occurred. It is also noted that one test lasts almost 400 h longer than the other, which is an example of the kind of variability in material performance during creep exacerbated by the fact these were accelerated creep tests.

The strain fields measured using DIC for specimen N-1 have been shown for t = 0 h, t = 97 h ($t/t_f = 0.5$) and t = 135 h. These times have been represent the period before creep occurred, halfway through the test and a few hours before a crack became visible by the naked eye respectively. Similar strain fields for specimen N-2, obtained using DIC, are displayed for t = 0 h, t = 180 h and t = 356 h. The latter has accumulated more strain overall as it crept for a longer period of time.

In this work, the limitations of the experimental apparatus meant that only one notch could be focused on, therefore the difference in strain fields between the two notches could not be quantified. However, as large-scale cracking initiated at one notch, it is possible that there was an asymmetric strain field produced prior to this. This would support prior work by (Gariboldi et al., 2016) on aluminium showing that although the initial strain field may have symmetry, strain can eventually accumulate more at one notch over the other.

To investigate the consistency in behaviour prior to large-scale cracking, Fig. 11 has plotted measurements of strain along the throat of the notch for both notched specimens of Alloy 617 at 97 h and 135 h into each. At both time points there is good consistency between the two specimens of Alloy 617, although N-2 has more strain close to the notch root at t = 97 h. Subsequently the behaviour differs between the two as the crack appears in one notch of N-1 soon afterwards. This early cracking of one specimen compared to the other could be an example of material variability in creep.

As previously detailed in Fig. 4, specimen N-1 had an array of ACPD probes welded over the entire length of its gauge region, while specimen N-2 had one set attached at the notch and one set located at a distance of 20 mm away to provide a remote field measurement. Results are shown for both specimens in Fig. 10, expressed using the normalised resistance ratio (ξ). There is clearly a diminishing resistance response as the distance from the notch increases. However, it can be seen that after 6 mm, there is no immediately visible increase in the gradient of the creep curve at the end of the steady-state portion of the graph. This is to be expected, as the resistance change is geometry driven until tertiary creep (Madhi and Nagy, 2011a; 2011b) and the presence of an elastic stress field further away from the notch means that strain increases are negligible in comparison to the near-notch region. The set of probes located 6 mm away from the notch is close enough to it to detect the strain localisation and crack formation occurring here. Finally, the resistance ratio is shown to accelerate well in advance of the visible crack formation, supporting previous experiments conducted (Davies et al., 2011) that show the ability of the

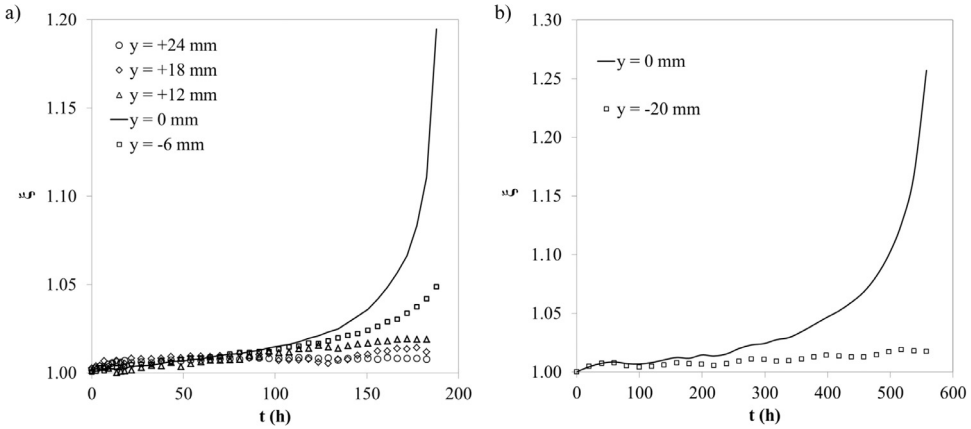

Fig. 10. Normalised resistance ratio (ξ) against time obtained using ACPD probes for a) Specimen N-1 with results shown at the centreline (solid line) and at distances of 24 mm (circles), 18 mm (diamonds), 12 mm (triangles)and 6 mm (squares) from it and b) Specimen N-2 with results shown at the centreline (solid line) and 20 mm away from it (squares).

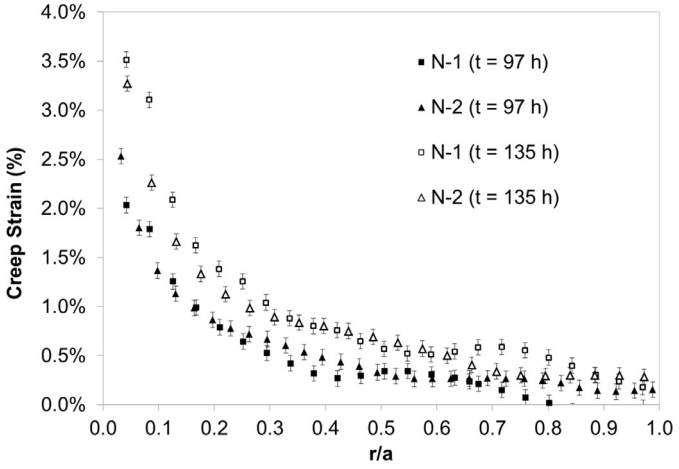

Fig. 11. Creep Strain measured using DIC along throat of notched Alloy 617 specimens at 97 h (solid squares for specimen N-1 and solid triangles for specimen N-2) and 135 h (hollow squares for specimen N-1 and hollow triangles for specimen N-2) into the test.

ACPD sensor to sense the onset of the accelerated portion of the material life in advance of conventional strain measurement tools.

6. Comparison with finite element model

Fig. 12 compares experimental results for specimen N-2 to predicted results from FE simulations at four different time points. It is seen that in the early stages there is a discrepancy between the FE and the experimental results. This is expected as the average creep strain rate method represents the entire creep curve using one constant strain rate. Therefore predictions using the model underestimate creep strain due to the initial high strain rate of primary creep. As time progresses, the discrepancy reduces until final failure of the model at t = 236 h, where failure has been defined in this case as the point of time when the first element becomes fully damaged according to Eq. (4). This is an important observation as failure will occur within the tertiary creep regime and therefore if the model can accurately match with experimental data at later points in the test it means that it remains suitable for use on this material.

7. Discussion

Creep constants for Alloy 617 have been calculated and presented using data from six tests to provide preliminary data for finite element modelling. Recent work performed by Knezevic et al. (2013) is plotted alongside data presented in this paper (see Fig. 7). It is seen that both data sets have a reasonable fit with each other. Any discrepancy may be due to differences in prior heat treatment between the two sets of material concerned. Knezevic et al considered two different annealing treatments whereas the material used within this research had been subject to a different annealing cycle before being thermally aged for 17000 hours. As mentioned earlier, alloy 617 shows an improvement in tensile properties after exposure to temperature for an extended period of time (Mankins et al., 1974), while for other materials the effect of thermal ageing is detrimental to creep resistance (Sklenička et al., 2015). Hence, it may be that the ageing process has affected the creep properties.

Notched specimens were tested to visualise creep deformation at elevated temperatures under multiaxial loading conditions as well as to compare with FE models. The first point to note is that both specimens deform in a similar manner, with the strain along the notch throat being similar in magnitude at 97 and 135 hours into the tests (see Fig. 11). Nevertheless, it is noted that although promise has been shown, more specimens must be tested to reduce the uncertainty.

Comparisons with FE models were performed. The FE combined an average creep strain rate analysis with a calibrated Cocks & Ashby damage model and results show a reasonable amount of agreement with experimental results. Discrepancies may be either due to inherent material variability or a requirement for more uniaxial creep test data to be obtained and analysed in order to further refine the material properties.

The ACPD sensor shows that the strain is highly localised as expected as the stress is localised at the notch tip. This observation is supported by strain fields in Figs. 8 and 9. Nevertheless, probes centred around a point 6 mm from the defect have detected acceleration showing some sensitivity of the sensor in this configuration when a stress raiser is in its vicinity.

8. Conclusions

Tests have been performed to characterise Alloy 617 at 700 °C. Tensile properties stated are consistent with previous literature values in Inconel alloy 617. Six creep tests have been performed at various stresses to provide creep data, which has been listed in

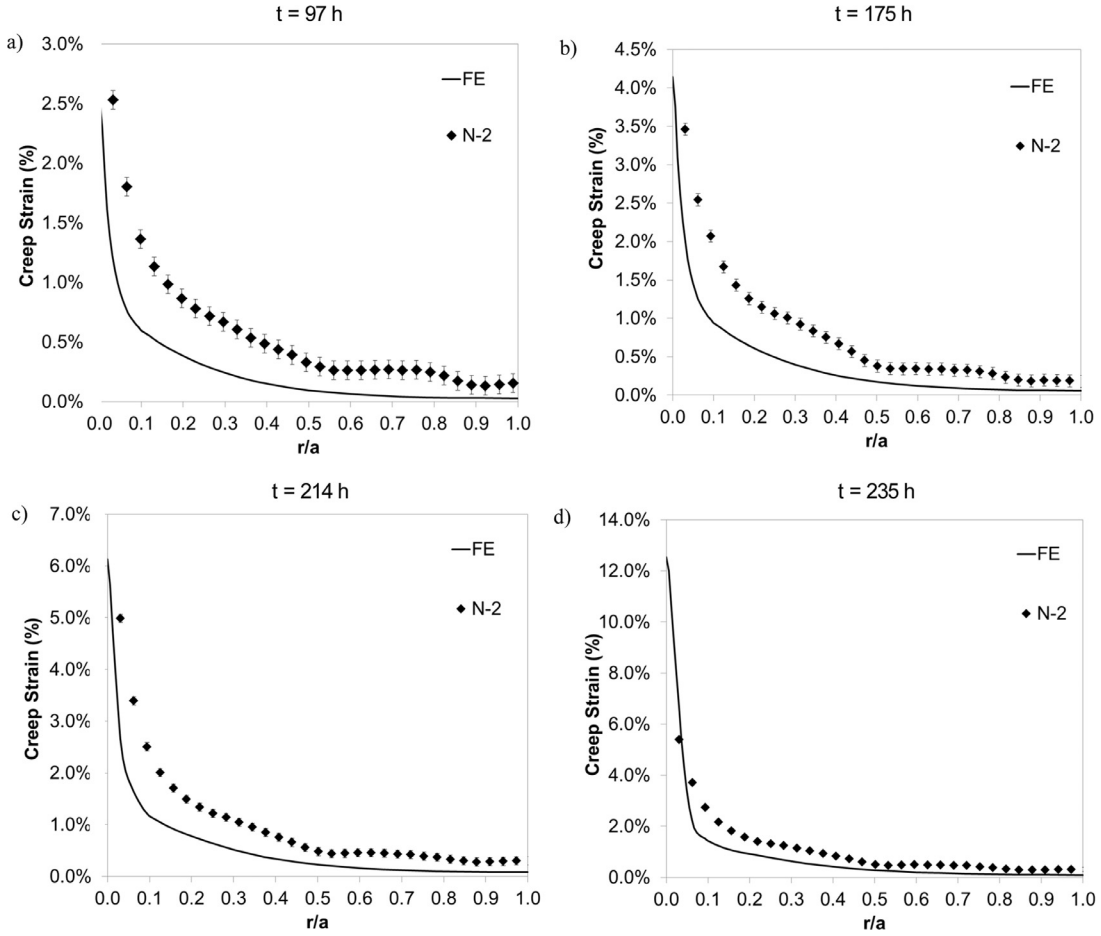

Fig. 12. Comparison between FE and creep strain along throat of specimen N-2 at a) t = 97 h, b)t = 175 h, c) t = 214 h, d) t = 236 h.

Table 5. Experiments are detailed that use DIC to map the strain fields of a specimen undergoing creep. Notched specimens have been tested to investigate the field evolution with respect to multiaxiality. Finite Element models using average creep rate properties from this data set have shown good agreement with experiments, with the quality of agreement increasing as time progresses.

The ACPD sensor shows promise for operation on specimens subject to 700 °C. The presence of a defect may be detected from up to 6 mm away, and may be increased if the current sensor electronics or configuration is adjusted to suit.

Testing is ongoing in order to better evaluate the behaviour of the alloy over a greater range of test stresses and lifetimes. However, values stated here are used to provide a reasonable characterisation of its material properties. In future, it will be necessary to extend the work on to other aspects of creep behaviour including its response to multiaxial stress states (i.e. using notched bars) and with regards to creep crack growth (CCG), for example using compact tensions (CT) specimens.

Acknowledgements

Dr Aditya Narayanan's PhD research at Imperial College London was supported by an EPSRC Case Studentship with E.ON. This research was also supported by EU project COMTES 700 [RFC-CP-04003]; and the European Community's Research Fund for Coal and Steel (7FP) under the MACPLUS project [ENER/FP7EN/249809/MACPLUS]. The help and advice of Dr Joseph Corcoran, Dr Keith Tarnowski, Professor Peter Nagy and Professor Peter Cawley FRS is very much appreciated in the development and application of the ACPD sensor. In addition, Professor Martyn Pavier and Dr Mahmoud Mostafavi are acknowledged for their invaluable support during thoughtful discussions about the research.

References

ASTM International, 2005. E633-00: Standard guide for use of thermocouples in creep and stress-Rupture testing to 1800 °F (1000 °C) in air. Annu. B. ASTM Stand. 2005 i (Reapproved).

Bhadeshia, H., Honeycombe, R., 2011. Steels: Microstructure and properties: microstructure and properties, Third ed. Elsevier Science.

Cocks, A.C.F., Ashby, M.F., 1982. On creep fracture by void growth. Prog. Mater. Sci. 27 (27), 189–244.

Davies, C.M., Nagy, P.B., Narayanan, A., Cawley, P., 2011. Continuous creep damage monitoring using a novel potential drop technique. In: ASME Press. Vessel. Pip. Conf.. ASME, Baltimore.

Evans, R.W., Wilshire, B., 1993. Introduction to creep, first ed. Maney Publishing.

Gariboldi, E., Naumenko, K., Ozhoga-Maslovskaja, O., Zappa, E., 2016. Analysis of anisotropic damage in forged Al-Cu-Mg-Si alloy based on creep tests, micrographs of fractured specimen and digital image correlations. Mater. Sci. Eng.: A 652, 175–185. http://dx.doi.org/10.1016/j.msea.2015.11.090.

Inconel alloy 617, 2005. Accessed 16/11/2013.

Kim, N.-H., Oh, C.-S., Kim, Y.-J., Davies, C.M., Nikbin, K., Dean, D.W., 2013. Creep failure simulations of 316h at 550 °C: part II: effects of specimen geometry and loading mode. Eng. Fract. Mech. 105, 169–181. doi:10.1016/j.engfracmech.2013.04.001.

Klöwer, J., Husemann, R., Bader, M., 2013. Development of nickel alloys based on alloy 617 for components in 700 °C power plants. Procedia Eng. 55, 226–231. doi:10.1016/j.proeng.2013.03.247.

Knezevic, V., Schneider, A., Landier, C., 2013. Creep behaviour of thick-Wall alloy 617 seamless pipes for 700 °C power plant technology. Procedia Eng. 55, 240–245. doi:10.1016/j.proeng.2013.03.249.

Madhi, E., Nagy, P.B., 2011. Geometrical gauge factor of directional electric potential drop sensors for creep monitoring. In: Thompson, D.O., Chimenti, D.E. (Eds.), AIP Rev. Prog. Quant. Nondestruct. Eval.. American Institute of Physics, pp. 1623–1630. doi:10.1063/1.3592123.

Madhi, E., Nagy, P.B., 2011. Material gauge factor of directional electric potential drop sensors for creep monitoring. In: Thompson, D.O., Chimenti, D.E. (Eds.), AIP Rev. Prog. Quant. Nondestruct. Eval.. American Institute of Physics, pp. 1233–1240. doi:10.1063/1.3592075.

Madhi, E., Nagy, P.B., 2011. Sensitivity analysis of a directional potential drop sensor for creep monitoring. NDT E Int. 44 (8), 708–717. http://dx.doi.org/10.1016/j.ndteint.2011.08.001.

Mankins, W.L., Hosier, J.C., Bassford, T.H., 1974. Microstructure and phase stability of INCONEL Alloy 617. Metall. Trans. 5 (12), 2579–2590. doi:10.1007/bf02643879.

Mehmanparast, A., Davies, C.M., Webster, G.A., Nikbin, K.M., 2014. Creep crack growth rate predictions in 316h steel using stress dependent creep ductility. Mater. High Temp. 31 (1), 84–94. doi:10.1179/0960340913Z.00000000011.

Oh, C.-S., Kim, N.-H., Kim, Y.-J., Davies, C., Nikbin, K., Dean, D., 2011. Creep failure simulations of 316H at 550 °C: part i: a method and validation. Eng. Fract. Mech. 78 (17), 2966–2977. doi:10.1016/j.engfracmech.2011.08.015.

Prajapati, S., Nagy, P.B., Cawley, P., 2012. Potential drop detection of creep damage in the vicinity of welds. NDT E Int. 47 (0), 56–65. doi:10.1016/j.ndteint.2011.11.014.

Sklenička, V., Kuchařová, K., Král, P., Kvapilová, M., Svobodová, M., Čmakal, J., 2015. The effect of hot bending and thermal ageing on creep and microstructure evolution in thick-walled p92 steel pipe. Mater. Sci. Eng.: A 644, 297–309. http://dx.doi.org/10.1016/j.msea.2015.07.072.

Spindler, M.W., 2004. The multiaxial creep ductility of austenitic stainless steels. Fatigue Fract. Eng. Mater. Struct. 27 (4), 273–281. doi:10.1111/j.1460-2695.2004.00732.x.

Xu, M., Chen, J., Lu, H., Xu, J., Yu, C., Wei, X., 2016. Effects of residual stress and grain boundary character on creep cracking in 2.25cr-1.6w steel. Mater. Sci. Eng.: A 659, 188–197. http://dx.doi.org/10.1016/j.msea.2016.02.025.

Yatomi, M., Bettinson, A.D., O'Dowd, N.P., Nikbin, K.M., 2004. Modelling of damage development and failure in notched-bar multiaxial creep tests. Fatigue Fract. Eng. Mater. Struct. 27 (4), 283–295. doi:10.1111/j.1460-2695.2004.00755.x.